Photothermal characteristics of gold nanoparticles of different size, shape, and composition: application in photothermal therapy

Gu Wei[1,2], Zhang Jinlan[1], Peng Liang[1], Cao Weiwu[1], Deng Haihua[1], Tao Wenquan[2]

(1. Wuhan Second Ship Design and Research Institute, Wuhan 430205, China;
2. Key Laboratory of Thermo-Fluid Science and Engineering of MOE, Xi′an Jiaotong University, Xi′an 710049, China)

Abstract: Due to its safety and high efficiency, photothermal therapy has been actively explored as minimally invasive approach to cancer therapy. The selection of nanoparticles to achieve photo thermal conversion efficiently is based on the absorption properties of the nanoparticles. Finite difference time domain method (FDTD) was used to calculate spectral absorption efficiencies for seven common types of gold nanoparticles: nanospheres, nanoshells, nanorods, nanosheets, nanocages, nanostars, and nanoflowers. The calculated results clearly demonstrate the dependence of absorption efficiencies and resonance wavelengths on the geometrical parameters of the nanoparticles. Via the volume absorption efficiencies, photothermal performance of the seven types of gold nanoparticles is compared quantitatively. The gold nanosheets are proved to offer the most superior photothermal performance in the near-infrared region (NIR) among the seven types of nanoparticles. From the vector distributions of the electric current densities, it is clearly shown that the resonant electric currents in the gold nanoparticles play the major role on the ultra large absorption cross-section in the NIR.

Key words: photothermal therapy; gold nanoparticles; absorption efficiencies; near-infrared region
CLC number: R730.57 **Document code: A** **DOI:** 10.3788/IRLA201847.1121005

不同尺寸、形状和组成的金纳米颗粒的光热特性：在癌症治疗中的应用

谷 伟[1,2],张锦岚[1],彭 亮[1],曹为午[1],邓海华[1],陶文铨[2]

(1. 武汉第二船舶设计研究所,湖北 武汉 430205;
2. 西安交通大学 热流科学与工程教育部重点实验室, 陕西 西安 710049)

摘 要: 光热疗法由于其安全和高效的优点，作为一种非破坏性方法在癌症治疗中有广泛的应用前景。光热疗法中,所采用的纳米颗粒在近红外波段的光热转换效率取决于纳米颗粒的光谱吸收特性。采用时域有限差分法对球型、壳型、杆型、片型、笼型、星型和花型等七种不同金纳米颗粒的光谱吸收特性进行了仿真计算，结果表明纳米颗粒的几何参数和结构对其光谱吸收效率和共振波长产生了显著的影响。通过对比七种金纳米颗粒的体积吸收系数,发现金纳米片在近红外波段的光热转换效率优于其他六种金纳米颗粒。从电流密度矢量分布得出,金纳米颗粒内部产生共振电流是导致金纳米颗粒在近红外波段具有明显的单色吸收特性的原因。

关键词: 光热治疗； 金纳米颗粒； 吸收效率； 近红外光

收稿日期:2018-06-05； **修订日期**:2018-07-08

基金项目:国家自然科学基金(51136004)

作者简介:谷伟(1986-),男,工程师,博士,主要从事微纳米结构材料光学特性方面的研究。Email:guwei.nht@hotmail.com

0 Introduction

Cancer has been one of the major threats to the lives of human beings for centuries[1]. Photothermal therapy, also known as photothermal ablation or hyperthermia, has been actively explored as minimally invasive approach to cancer therapy[2]. It is a procedure based on localized heating due to light absorption for selective destruction of abnormal cells[3]. Near-infrared light(700−1 100 nm) is preferred for such an application, as most biological soft tissues have a relatively low light absorption coefficient in the NIR regions[4], known as the tissue optical window or therapeutic window. The key components of this technique are phototherapeutic transducers that can absorb and convert NIR light into heat through a nonradiative mechanism with high efficiency[5-6]. There are two levels of "selectivity" in photothermal therapy: (1) the well-engineered phototherapeutic transducers could selectively target tumor via either passive or active tumor homing[7-14]; (2) the light illumination could be spatially controlled to irradiate only the diseased lesion without damaging normal tissues. A combination of these two benign moieties (phototherapeutic agents and NIR light) allows a noninvasive delivery of heat to a tumor volume by using an extracorporeal, low-power diode laser to induce a photothermal destruction of the tumor embedded with photothermal transducers[15]. The schematic diagram of photothermal therapy is given by Fig.1.

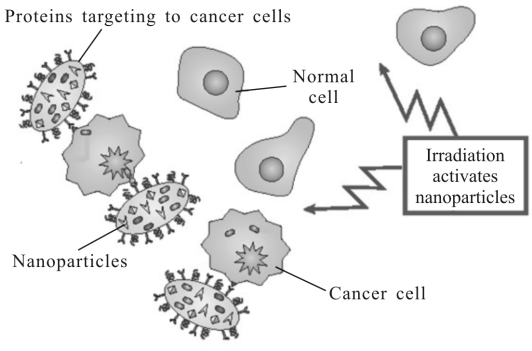

Fig.1 Schematic diagram of photothermal therapy

Over the past decade, many different types of photothermal transducers have been reported. Due to the reasonable biocompatibility, gold, a rather inert element, has been widely used to construct different shape of nanoparticles including gold nanospheres[3], gold nanoshells[15-18], gold nanorods[7,9,19-21], gold nanosheets[22,23], gold nanocages[10,24,25], gold nanoflowers[26], and gold nanostars[27-29]. To minimize tumor recurrence, efficient delivery of the nanoparticles to the entire tumor region is critical in order to ensure cytotoxic temperature everywhere in the tumor[21]. To reach this goal, two key points must be noted when designing the nanoparticles[30]: (1) the size of nanoparticles should be as small as possible in consideration of nanoparticle uptake and retention by cells and tissue; (2) the absorption cross-section of nanoparticles in the NIR regions should be as large as possible to convert NIR light to heat effectively.

Although many different types of gold nanoparticles have been designed, and their excellent photothermal performance in NIR regions has been demonstrated in vitro or in vivo[3,7,9,10,15-29], works on comprehensive comparison of different types of nanoparticle are still very little. Besides, the reasons behind the spectral control of absorption cross-section for the previous mentioned gold nanoparticles are still not explained clearly. In this paper, we will conduct a comprehensive and quantitative comparison of seven common different types of gold nanoparticles, as shown in Fig.2, and reveal the mechanisms that result

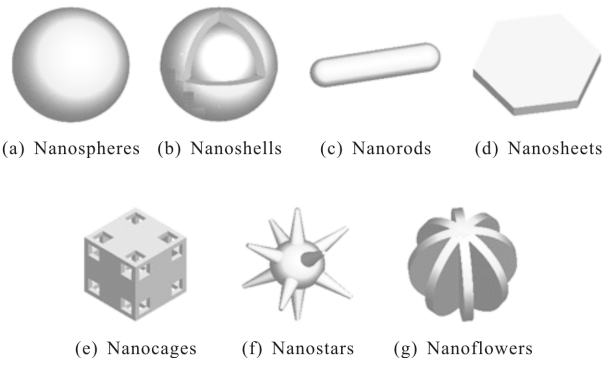

Fig.2 Seven types of gold nanoparticles

in very large monochromatic absorption cross-sections. The works of this paper may be helpful for designing new type of nanoparticles with good photothermal performance.

1 Methodology

The photothermal performance of gold nanoparticles can be quantified in terms of absorption efficiency Q_{abs} and optical resonance wavelength λ_{max}. In general, the characteristic dimensions of nanoparticles in photothermal therapy are comparable with or smaller than the wave lengths of NIR lights, so an electrodynamic method, finite difference time domain (FDTD) method, is used to compute the optical properties of nanoparticles accurately. The absorption efficiency Q_{abs} is defined as the ratio of energy absorption cross-section to the geometirc cross-sectional area of the particle. It is common to specify the size of a particle of an arbitrary shape and volume V in terms of an effective radius given by:

$$r_{eff}=(3V/4\pi)^{1/3} \quad (1)$$

Thus, the cross-sectional area of the particle with arbitrary shape is πr_{eff}^2. By defining effective radius, absorption efficiencies Q_{abs} of particles with different shapes can be compared quantitatively.

The ideal photothermal particles should have small effective radius r_{eff} and large absorption efficiency Q_{abs} in the NIR region, since particles of smaller size can be loaded in a given volume with a greater number than particles of larger size. In view of this, the volumetric absorption coefficient $\mu_\alpha=Q_{abs}/r_{eff}$ is adopted as the criterion of photothermal performance. The μ_α is expressed in units of μm^{-1}, and have the same physical mean with C/V where C is the absorption cross-section and V is the volume of the particle. Larger value of μ_α means that more NIR light is absorbed and then more heat is generated by the particles of the same occupied space volume.

Before studying and comparing the optical properties of the seven types of gold nanoparticles, the accuracy of FDTD is firstly demonstrated. The dependence of resonant wavelength that has the most energy absorbed by gold nanorods (Fig.2 (c)) on the aspect ratios (Length/Width) is shown in Fig.3, where the black square dots line corresponds to the results computed by FDTD method and red circle dots line corresponds to the experiment data from Ref.[31]. It can be seen that the results computed by FDTD method agree with the experiment data very well.

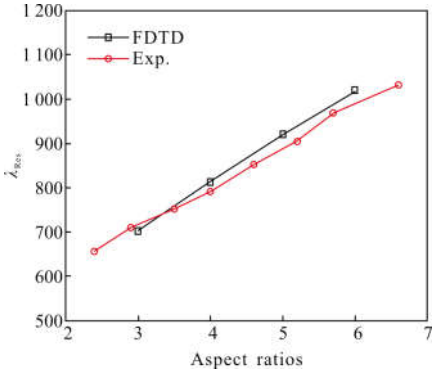

Fig.3 Dependence of λ_{Res} on the aspect ratios of gold nanoparticles

2 Results and discussion

2.1 Gold nanospheres

Because of easily manufacturing, gold nanospheres are of the most common nanoparticles used in photothermal therapy. Figure 4 gives the calculated spectral Q_{abs} for gold nanospheres of

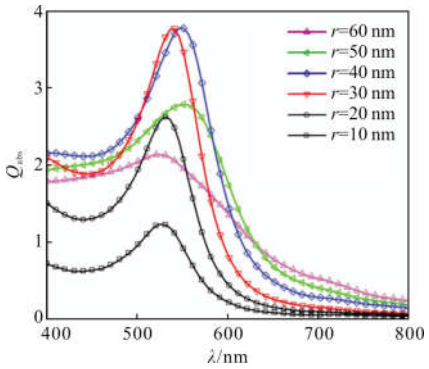

Fig.4 Spectral absorption efficiency of gold nanospheres of different radius

different radius (r=10, 20, 30, 40, 50, 60 nm). It can be seen that the Q_{abs} reach maximum around λ=540 nm, and will be depressed by increasing r if r>30 nm.

That is because most of energy is scattered for larger r. Furthermore, the wave length $\lambda_{max,abs}$, which corresponds to the largest Q_{abs}, stays around 540 nm and is difficult to be shifted to NIR range via changing the radius.

2.2 Silica-gold nanoshells

Gold nanoshells are composed of core part and shell part, as shown in Fig.2(b). The material of core part is usually dielectric, like SiO_2, and shell part is gold [2]. If the inner radius and external radius are denoted by r_1 and r_2, respectively, the structure of nanoshells can be well described by the ratio $\alpha=r_1/r_2$ and external radius r_2.

Figure 5(a) and (b) give the influence of structure parameters α and r_2 on Q_{abs}, respectively. We can see that the $\lambda_{max,abs}$ is able to be shifted from visible to NIR region via increasing α when r_2 is fixed. However, the peak of Q_{abs} will be cut off when α is larger than 0.9. That is because the thickness of shell is smaller than 3 nm for $\alpha>0.9$ when r_2=30 nm, which is too thin to stimulate the SPR. Figure 5 (b) shows that the $\lambda_{max,abs}$ is hardly influenced by r_2 when α is fixed. Furthermore, Q_{abs} will be diminished for larger r_2, because scattering effect is enhanced by increasing r_2, which is the same with nanoshperes.

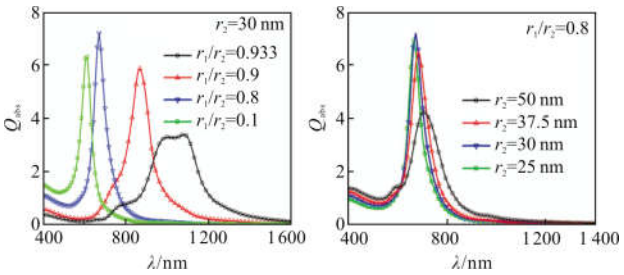

(a) r_2=30 nm and different α (b) α=0.8 nm and different r_2

Fig.5 Spectral Q_{abs} for different structure parameters of r_2 or α

2.3 Gold nanorods

The geometrical parameters of gold nanorods include radius r and aspect ratio α. Figure 6(a) and (b) show the influence of α and r on Q_{abs} respectively. It can be seen that $\lambda_{max,abs}$ will be shifted form visible region to NIR region with the increasing of α when r is fixed, and the maximum of Q_{abs} will be enhanced for larger α. However, $\lambda_{max,abs}$ is independent on r if α is fixed, but the maximum of Q_{abs} can be further enhanced via larger r.

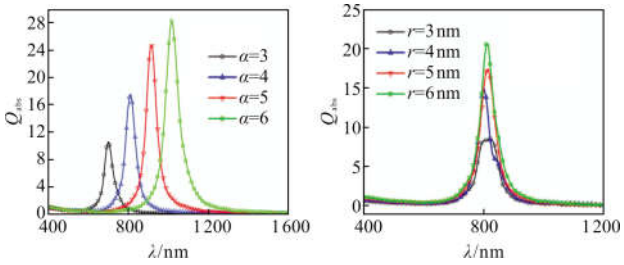

(a) r=5 nm with different α (b) α=4 with different r

Fig.6 Spectral Q_{abs} of different structure parameters of r or α with electric field parallel to the nanorod

2.4 Gold nanosheets

The size of gold nanosheets can be determined by side length l of the hexagon and thickness t. It is found from Fig.7(a) and (b) that both l and t are able to change $\lambda_{max,abs}$ and Q_{abs}. Via enlarging l, the maximum of Q_{abs} can be increased, and $\lambda_{max,abs}$ is able to be shifted from visible region to NIR region. On the other hand, the maximum of Q_{abs} can be increased, and $\lambda_{max,abs}$ is able to be shifted from visible region to NIR region by diminishing t.

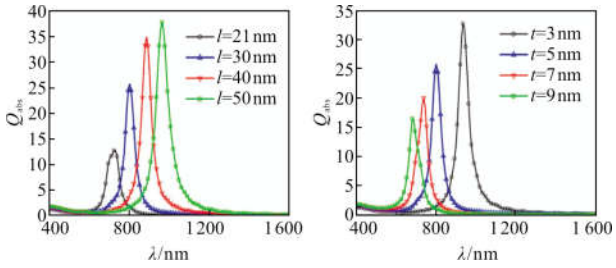

(a) t=5 nm for different l (b) l=30 nm for different t

Fig.7 Spectral Q_{abs} of different structure parameters of l or t with incident light perpendicular to the surface of the nanosheet

2.5 Gold nanocages

The structure of nanocages are shown in Fig.2(e), and can be described by the length l and thickness t, as depicted in Fig.8. Figure 9 (a) and (b) give the influence of structure parameters l and t on Q_{abs} respectively. It shows that both l and t can control the location of $\lambda_{max,abs}$. Via increasing l, the $\lambda_{max,abs}$ will be shifted to long wave region when the t is fiexed. On the other hand, the $\lambda_{max,abs}$ will be shifted to short wave

region by increasing t when l is fixed. However, both l and t do not influence the maximum of Q_{abs} obviously.

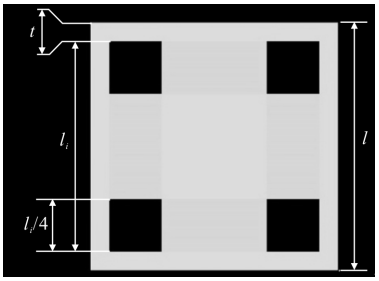

Fig.8 Structure parameters of nanocages

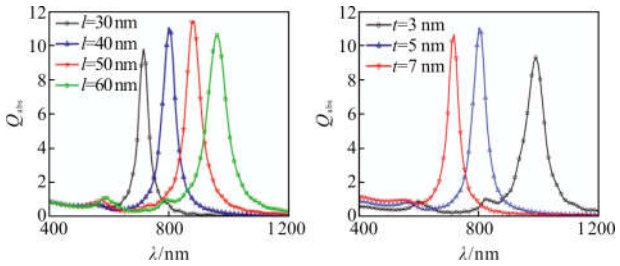

(a) t=5 nm with different l (b) l=40 nm with different t

Fig.9 Spectral Q_{abs} of different structure parameters of l or t

2.6 Gold nanostars

Gold nanostars are constructed by growing stabs on the surface of nanospheres, as shown in Fig.2(f). We just consider the cases of core radius r_c=12 nm and top radius of stabs r_t=2 nm, and study the influence of the length l and bottom radius rb of stabs on Q_{abs}. It can be seen from Fig.10(a) and (b) that the $\lambda_{max,abs}$ can be shifted to longer wave region by increasing l when r_b is fixed, or by decreasing r_b when l is fixed, and the Q_{abs} reaches maximum when l=17.5 nm and r_b=5 nm.

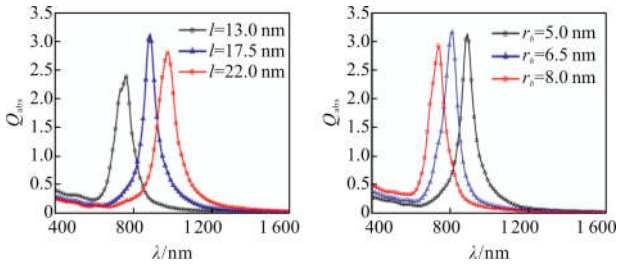

(a) r_b=5 nm with different l (b) l=17.5 nm with different r_b

Fig.10 Spectral Q_{abs} of different structure parameters of l or r_b

2.7 Gold nanoflowers

The nanoflower is constructed by intersecting four orbicular sheets, and the angle between the neighbor two orbicular sheets is 45°, as shown in Fig.2 (g). The structure parameters of nanoflowers include the radius r and the thickness t of the orbicular sheets. As shown in Fig.11 (a), the $\lambda_{max,abs}$ can be shifted by varying t with r fixed, but the maximum of Q_{abs} changes little. However, the maximum Q_{abs} can be further increased by enlarging r, accompanied by $\lambda_{max,abs}$ shifted to longer wave region, as shown in Fig.11(b).

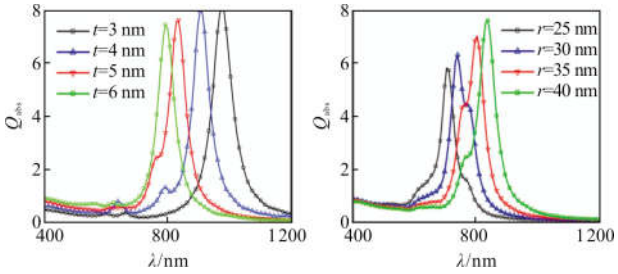

(a) r=40 nm with different t (b) t=5 nm with different r

Fig.11 Spectral Q_{abs} of different structure parameters of t or r

2.8 Comparison of seven shapes of gold nanoparticles

The calculated wavelengths $\lambda_{max,abs}$ and volume absorption coefficients μ_α (at wave length $\lambda_{max,abs}$) for the seven types of nanoparticles of different dimensions have been tabulated in Tab.1. We can clearly see that the values of μ_α of gold nanosheets and gold nanorods are comparable and obviously larger than that of the other five types of gold nanoparticles. Therefore, the order of the photothermal performance in NIR region of these seven types of gold nanoparticles should be: gold nanosheets ≈ gold nanorods > gold nanocages > gold nanoflowers > gold nanoshells>gold nanostars>gold nanospheres.

In order to further explore the mechanisms, which result in the very large of Q_{abs} at nearly monochromatic wavelengths, the vectors of the electric current density are calculated by

$$J=\sigma E \tag{2}$$

where J in $A\cdot m^{-2}$ is the current density; and σ in $A\cdot(V\cdot m)^{-1}$ is the electric conductivity. The σ is frequency-dependent, i.e.

Tab.1 Calculated wavelength $\lambda_{max,abs}$, volume absorption coefficient μ_α(at wavelength $\lambda_{max,abs}$) for the seven types of nanoparticles

Nanoparticle type	Dimensions/nm	r_{eff}/nm	$\lambda_{max,abs}$/nm	μ_α/μm^{-1}
Nanospheres	r=10	10	526	123.30
Nanospheres	r=20	20	531	131.23
Nanospheres	r=30	30	541	125.60
Nanospheres	r=40	40	551	94.41
Nanospheres	r=50	50	551	55.75
Nanospheres	r=60	60	526	35.59
Nanoshells	r_1=20, r_2=25	25	667	277.96
Nanoshells	r_1=21, r_2=30	30	616	210.47
Nanoshells	r_1=24, r_2=30	30	672	240.49
Nanoshells	r_1=27, r_2=30	30	870	195.85
Nanoshells	r_1=28, r_2=30	30	1 086	113.311
Nanoshells	r_1=30, r_2=37.5	37.5	681	172.22
Nanoshells	r_1=40, r_2=50	50	703	84.98
Nanorods	r=3.5, α=4	6.18	815	1 487.12
Nanorods	r=3, α=4	5.30	822	1 620.98
Nanorods	r=4, α=4	7.06	801	2 132.20
Nanorods	r=5, α=3	7.94	702	1 334.46
Nanorods	r=5, α=4	8.83	815	1 981.29
Nanorods	r=5, α=5	9.56	921	2 573.81
Nanorods	r=5, α=6	10.20	1 019	2 767.58
Nanorods	r=6, α=4	10.59	808	1 943.60
Nanosheets	l=21, t=5	11.10	731	1 154.19
Nanosheets	l=30, t=3	11.88	935	2 754.03
Nanosheets	l=30, t=5	14.08	801	1 828.48
Nanosheets	l=30, t=7	15.75	738	1 268.19
Nanosheets	l=30, t=9	17.13	681	960.28
Nanosheets	l=40, t=5	17.06	885	2 044.94
Nanosheets	l=50, t=5	19.80	963	1 905.23
Nanocages	l=30, t=5	18.61	717	527.21
Nanocages	l=40, t=3	24.81	991	376.03
Nanocages	l=40, t=5	24.81	801	446.33
Nanocages	l=40, t=7	24.81	717	429.67
Nanocages	l=50, t=5	31.02	885	367.96
Nanocages	l=60, t=5	37.22	963	285.58
Nanostars	l=13, r_b=5, r_t=2, r_c=12	27.00	780	88.63
Nanostars	l=17.5, r_b=3.5, r_t=2, r_c=12	31.50	1 068	67.61
Nanostars	l=17.5, r_b=5, r_t=2, r_c=12	31.50	892	83.25
Nanostars	l=17.5, r_b=6.5, r_t=2, r_c=12	31.50	808	76.80
Nanostars	l=17.5, r_b=8, r_t=2, r_c=12	31.50	752	62.70
Nanostars	l=22, r_b=5, r_t=2, r_c=12	36.00	1 019	67.71
Nanoflowers	r=25, t=5	25.00	703	233.40
Nanoflowers	r=30, t=5	30.00	738	210.85
Nanoflowers	r=35, t=5	35.00	801	201.31
Nanoflowers	r=40, t=3	40.00	977	203.55
Nanoflowers	r=40, t=4	40.00	907	200.09
Nanoflowers	r=40, t=5	40.00	836	190.67
Nanoflowers	r=40, t=6	40.00	794	186.32

$$\sigma=\sigma'+i\sigma''=-i\omega\varepsilon \tag{3}$$

where ε in $C\cdot(V\cdot m)^{-1}$ is the electric permittivity of the gold; and ω is the frequency of the incident light.

Note that Eq.(2) gives the complex vector of J, however, only Re (J) represents the actual current density, which can be expressed as the sum of the conduction current and displacement current, i.e.

$$\mathrm{Re}(J)=J_{cond}+J_{disp}=\sigma'\mathrm{Re}(E)-\sigma''\mathrm{Im}(E) \tag{4}$$

Figure 12(a) and (b) plot the distributions of the electric current density of gold nanorods (r=5 nm, α=6) for the incident wave length of λ=1 019 nm and λ=780 nm respectively. As listed in Tab.1, λ=1 019 nm results in the maximum Q_{abs}. We can see that there exist extraordinarily large electric currents, when Q_{abs} reaches maximum, and a shape of half wave is exactly constructed by the surface current density, which is known as the surface plasma resonances (SPR). However, no resonant electric currents are observed in the gold nanorods for λ=780 nm, where Q_{abs} is much small. The same phenomenon is found for gold nanosheets as depicted Fig.13 (a) and (b). Hence, it is believed that stimulating resonant electric current in the gold nanoparticles can enhance the absorption efficiency dramatically.

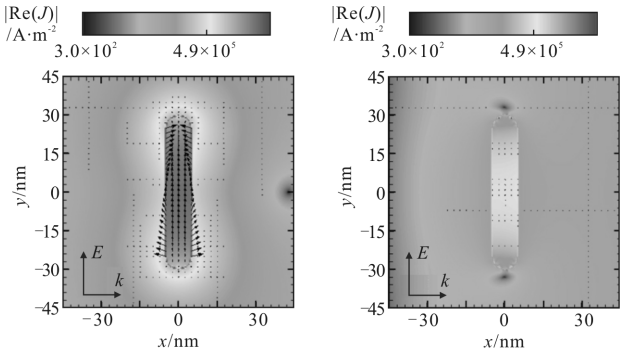

Fig.12 Distribution of the electric current density of gold nanorods (r=5 nm, α=6, colors for absolute values |Re(J)|, and arrows for vectors Re(J))

To further confirming this, we calculated the absorption efficiencies of gold nanosheets for the two cases as shown in Fig.14 (a) and (b). The directions of incident light are parallel to the surface of the gold

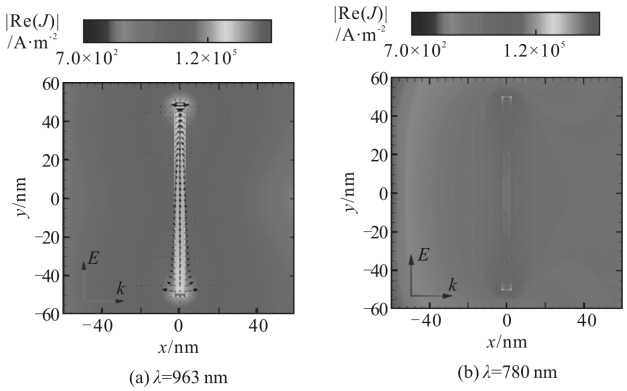

Fig.13 Distribution of the electric current density and electric fields of gold nanosheets(l=60 nm, t=5 nm, colors for absolute values |Re(J)|, and arrows for vectors Re(J)).

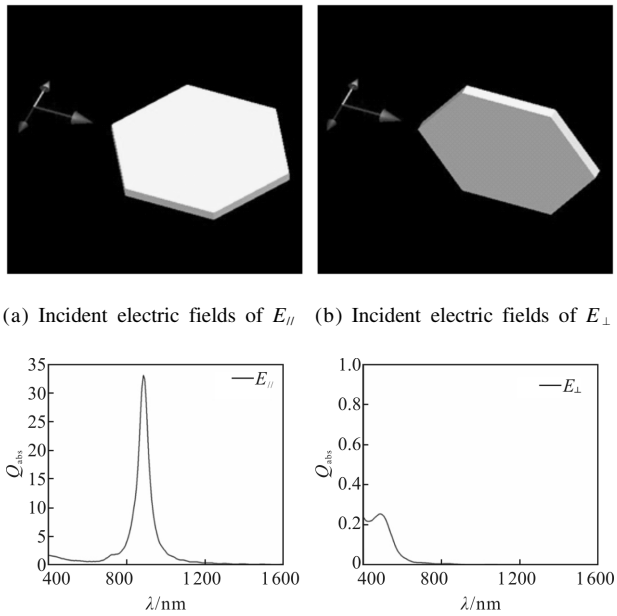

Fig.14 Influence of the direction of incident electric field on Q_{abs}

nanosheets for both of these two cases, but the directions of the electric fields are different. The electric fields in Fig.14 (a) and (b) are respectively parallel ($E_{//}$) or perpendicular to ($E_{\perp}$) the surface of the gold nanosheets. For these two cases, the Q_{abs} are very different. For the case of $E_{//}$, the induced electric currents in gold nanosheets are also parallel to the surface, so the resonant electric currents can be stimulated along the surface of gold nanosheets for a specific λ, and sequentially lead to dramatically large Q_{abs}, as shown in Fig.14(c). However, for the case of $E_{\perp}$, the resonant electric currents are unable to be

stimulated because of the dimension restriction along the thick direction, and the Q_{abs} is much small for the considered wave region, as depicted in Fig.14(d).

By comparing the structures of the considered seven types of gold nanoparticles, we find that the flat-thin structures like nanosheet, nanocage (the walls) and nanoflowers or the slender-long structures like nanorods and nanostars (the stabs) can stimulate the resonant electric currents efficiently and then result in large Q_{abs}. Thus, the flat-thin structures and slender-long structures should be included in the nanoparticles to improve their absorption performance in NIR region.

3 Conclusion

To obtain a quantitative guide for selection and design of gold nanoparticles for photothermal-based applications in photothermal therapy, a systematic study of the variation of resonance wavelength $\lambda_{max,abs}$ and the absorption efficiency with nanoparticle dimensions was conducted for seven different types of gold nanoparticles , i.e., gold nanospheres, silica-gold nanoshells, gold nanorods, gold nanosheets, gold nanocages, gold nanostars, and gold nanoflowers. It was clearly demonstrated from the calculated spectral Q_{abs} that the absorption performance of nanoparticles in NIR region were highly dependent on the nanoparticle dimension and shape. Except for the gold nanospheres, the resonant $\lambda_{max,abs}$ of maximum Q_{abs} for all the other six gold nanoparticle types can be shifted in to NIR region by changing the particle′s dimensions. By comparing their volume absorption efficiency, we found that the order of the photothermal performance in NIR region of these seven types of gold nanoparticles is gold nanosheets ≈ gold nanorods > gold nanocages > gold nanoflowers > gold nanoshells > gold nanostars > gold nanospheres. From the vector distributions of the electric current density, it was found that it is the resonant electric currents stimulated in the nanoparticles that results in the ultra large Q_{abs}. The flat-thin structures and slender-long structures are suggested to be included in the nanoparticles to improve their absorption performance in NIR region.

References:

[1] Ferrari M. Cancer nanotechnology: opportunities and challenges [J]. ***Nat Rev Cancer***, 2005, 5 (3): 161-171.

[2] Cheng L, Wang C, Feng L, et al. Functional nanomaterials for phototherapies of cancer [J]. ***Chemical Reviews***, 2014, 114 (21): 10869-10939.

[3] Pitsillides C M, Joe E K, Wei X, et al. Selective cell targeting with light-absorbing microparticles and nanoparticles [J]. ***Biophysical Journal***, 2003, 84 (6): 4023-4032.

[4] Ritz J P, Roggan A, Isbert C, et al. Optical properties of native and coagulated porcine liver tissue between 400 and 2 400 nm [J]. ***Lasers in Surgery and Medicine***, 2001, 29(3): 205-212.

[5] Jain P K, El-Sayed I H, El-Sayed M A. Au nanoparticles target cancer [J]. ***Nano Today***, 2007, 2(1): 18-29.

[6] Boris K, Vladimir Z, Andrei M, et al. Optical amplification of photothermal therapy with gold nanoparticles and nanoclusters [J]. ***Nanotechnology***, 2006, 17 (20): 5167.

[7] Li Z, Huang H, Tang S, et al. Small gold nanorods laden macrophages for enhanced tumor coverage in photothermal therapy [J]. ***Biomaterials***, 2016, 74: 144-154.

[8] Wang Y, Black K C L, Luehmann H, et al. Comparison Study of gold nanohexapods, nanorods, and nanocages for photothermal cancer treatment [J]. ***ACS Nano***, 2013, 7(3): 2068-2077.

[9] Huang X, El-Sayed I H, Qian W, et al. Cancer cell imaging and photothermal therapy in the near-infrared region by using gold nanorods [J]. ***Journal of the American Chemical Society***, 2006, 128(6): 2115-2120.

[10] Yavuz M S, Cheng Y, Chen J, et al. Gold nanocages covered by smart polymers for controlled release with near-infrared light [J]. ***Nat Mater***, 2009, 8(12): 935-939.

[11] Kam N W S, O′Connell M, Wisdom J A, et al. Carbon nanotubes as multifunctional biological transporters and near-infrared agents for selective cancer cell destruction [J]. ***Proceedings of the National Academy of Sciences of the United States of America***, 2005, 102(33): 11600-11605.

[12] Hessel C M, Pattani V P, Rasch M, et al. Copper selenide nanocrystals for photothermal therapy [J]. ***Nano Letters***, 2011, 11(6): 2560-2566.

[13] Ni D, Ding H, Liu S, et al. Drug delivery: superior

intratumoral penetration of paclitaxel nanodots strengthens tumor restriction and metastasis prevention [J]. ***Small***, 2015, 11(21): 2465-2465.

[14] Tian B, Wang C, Zhang S, et al. Photothermally enhanced photodynamic therapy delivered by nano-graphene oxide [J]. ***ACS Nano***, 2011, 5(9): 7000-7009.

[15] Hirsch L R, Stafford R J, Bankson J A, et al. Nanoshell-mediated near-infrared thermal therapy of tumors under magnetic resonance guidance[J]. ***Proceedings of the National Academy of Sciences***, 2003, 100(23): 13549-13554.

[16] Loo C, Lin A, Hirsch L, et al. Nanoshell-enabled photonics-based imaging and therapy of cancer [J]. ***Technology in Cancer Research & Treatment***, 2004, 3(1): 33-40.

[17] Kim J, Park S, Lee J E, et al. Designed fabrication of multifunctional magnetic gold nanoshells and their application to magnetic resonance imaging and photothermal therapy [J]. ***Angewandte Chemie International Edition***, 2006, 45 (46): 7754-7758.

[18] Madsen S J, Baek S -K, Makkouk A R, et al. Macrophages as cell-based delivery systems for nanoshells in photothermal therapy [J]. ***Annals of Biomedical Engineering***, 2011, 40 (2): 507-515.

[19] Dickerson E B, Dreaden E C, Huang X H, et al. Gold nanorod assisted near-infrared plasmonic photothermal therapy (PPTT) of squamous cell carcinoma in mice [J]. ***Cancer Letters***, 2008, 269(1): 57-66.

[20] Huang X, Neretina S, El-Sayed M A. Gold nanorods: from synthesis and properties to biological and biomedical applications [J]. ***Advanced Materials***, 2009, 21(48): 4880-4910.

[21] Maltzahn G, Park J -H, Agrawal A, et al. Computationally guided photothermal tumor therapy using long-circulating gold nanorod antennas [J]. ***Cancer Research***, 2009, 69 (9): 3892-3900.

[22] Huang X, Tang S, Mu X, et al. Freestanding palladium nanosheets with plasmonic and catalytic properties [J]. ***Nat Nano***, 2011, 6(1): 28-32.

[23] Pelaz B, Grazu V, Ibarra A, et al. Tailoring the synthesis and heating ability of gold nanoprisms for bioapplications [J]. ***Langmuir***, 2012, 28 (24): 8965-8970.

[24] Skrabalak S E, Chen J, Sun Y, et al. Gold nanocages: synthesis, properties, and applications [J]. ***Accounts of Chemical Research***, 2008, 41(12): 1587-1595.

[25] Xia Y, Li W, Cobley C M, et al. Gold nanocages: from synthesis to theranostic applications [J]. ***Accounts of Chemical Research***, 2011, 44(10): 914-924.

[26] Tian Q W, Tang M H, Sun Y G, et al. Hydrophilic flower-like CuS superstructures as an efficient 980 nm laser-driven photothermal agent for ablation of cancer cells[J]. ***Advanced Materials***, 2011, 23(31): 3542-3547.

[27] Julien R G N, Delphine M, Frédéric L, et al. Synthesis of PEGylated gold nanostars and bipyramids for intracellular uptake[J]. ***Nanotechnology***, 2012, 23 (46): 465602.

[28] Yuan H, Fales A M, Vo-Dinh T. TAT peptide-functionalized gold nanostars: enhanced intracellular delivery and efficient NIR photothermal therapy using ultralow irradiance [J]. ***Journal of the American Chemical Society***, 2012, 134(28): 11358-11361.

[29] Yuan H, Khoury C G, Wilson C M, et al. In vivo particle tracking and photothermal ablation using plasmon-resonant gold nanostars [J]. ***Nanomedicine: Nanotechnology, Biology and Medicine***, 2012, 8(8): 1355-1363.

[30] Jain P K, Lee K S, El-Sayed I H, et al. Calculated absorption and scattering properties of gold nanoparticles of different size, shape, and composition: applications in biological imaging and biomedicine [J]. ***The Journal of Physical Chemistry B***, 2006, 110(14): 7238-7248.

[31] Huang X, El-Sayed M A. Gold nanoparticles: optical properties and implementations in cancer diagnosis and photothermal therapy [J]. ***Journal of Advanced Research***, 2010, 1(1): 13-28.